Force distribution in a granular medium under dynamic loading

Vyacheslav A. Danylenko,[1] Sergiy V. Mykulyak,[1,*] Volodymyr O. Polyakovskyi,[1] Vasyl V. Kulich,[1] and Ivan I. Oleynik[2]
[1]*Subbotin Institute of Geophysics, NASU, Kiev 03680, Ukraine*
[2]*Department of Physics, University of South Florida, Tampa, Florida 33620, USA*
(Received 8 July 2016; revised manuscript received 25 January 2017; published 28 July 2017)

Force distribution in a granular medium subjected to an impulse loading is investigated in experiment and computer simulations. An experimental technique is developed to measure forces acting on individual grains at the bottom of the granular sample consisting of steel balls. Discrete element method simulation also is performed under conditions mimicking those in experiment. Both theory and experiment display exponentially decaying maximum force distributions at the bottom of the sample in the range of large forces. In addition, the simulations also reveal exponential force distribution throughout the sample and uncover correlation properties of the interparticle forces during dynamic loading of the granular samples. Simulated time dependence of coordination number, orientational order parameter, correlation radius, and force distribution clearly demonstrates the nonequilibrium character of the deformation process in a granular medium under impulse loading.

DOI: 10.1103/PhysRevE.96.012906

I. INTRODUCTION

Mechanical properties of a granular medium differ from those of solids, liquids, or gases. The unusual behavior is caused by a complex mechanism of redistribution of forces inside the granular material upon application of an external load [1–3]. This force redistribution is transmitted through the sample via interparticle contacts. Unlike ordinary crystalline or polycrystalline solids, the interparticle contact forces are distributed inhomogeneously throughout the granular sample, resulting in abnormally large forces experienced by the walls of the container surrounding the medium, which might result in their irreversible damage. Therefore, the characterization of the force distribution in the granular medium is of great practical importance [4,5].

Several aspects of interparticle interactions in granular systems, such as distribution of forces between particles and force correlations, have been studied previously under static and slow shearing loads. For example, experimental photoelastic visualization [1,4,6–10] and computer simulations of the stress field distribution [11–14] have shown that the interparticle forces are distributed inhomogeneously in the volume of the sample forming a so-called "force chain" network, which can span the entire system. A series of experiments employing static compression [2,3,15,16] and slow shear [6,9,17] demonstrated that the distribution of interparticle forces has a bimodal character: It displays an exponential decrease for forces larger than the mean force, whereas it displays either a small peak or a plateau for the forces below the mean force. These features of the distribution function, confirmed by numerous two-dimensional (2D) and three-dimensional (3D) simulations [11,12,18–21], are due to the structure of the force network, which consists of two subnetworks. A "weak" subnetwork is formed of the particles experiencing the forces below the mean force and a "strong" subnetwork—of the particles with forces larger than the mean force, the latter being a small fraction of all forces [11]. The distribution of the contact forces has long-range correlations along the force chains and short-range correlations—in all other directions [14].

Several theoretical approaches have been proposed in the past to interpret interparticle force distributions [22–26]. However, most of them considered only granular systems under static conditions and measured the forces using sensitive carbon paper [2,3,15], photoelastic [4,8,27], and wavelength-scanning interferometric [28] methods. Sensors at the bottom of a container also have been used for force measurements [6,16]. However, due to substantial physical dimensions, the measured forces were averaged over a large number of particles. Similarly, *tactile* sensors were used in experiments with sand, which measured the forces exerted on a cluster of grains rather than on individual particles [29,30]. A number of experiments probing forces in 2D dynamic processes have been performed using samples in massifs consisting of photoelastic [1,6,7,9,31] and rubber disks [32]. In recent years, several techniques have been developed to measure interparticle forces directly inside 3D granular systems including confocal imaging [33,34], refractive index matched imaging [35,36], and x-ray tomography [37,38]. The first two techniques are purely optical as they use transparent particles. However, all three-dimensional experiments performed so far have been conducted under pure static conditions.

This paper bridges the gap in force characterization in the granular medium by investigating the force distribution in samples subjected to impulse loading. It is expected that the underlying phenomena under such strongly nonequilibrium conditions will be completely different from those observed during static or steady dynamic Couette shearing deformations [1]. The experiments measuring the forces at the bottom of the granular sample are supplemented by extensive computer modeling which allowed for uncovering force distribution inside the granular sample.

II. EXPERIMENTAL METHOD

A method for measuring forces under impulse loading experienced by individual particles at the bottom of the container has been developed and applied to perform detailed force characterization. The schematic of the experimental

*mykulyak@ukr.net

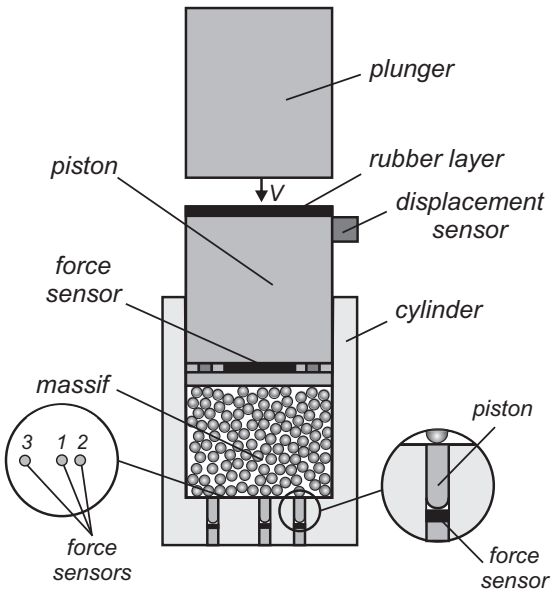

FIG. 1. A sketch of the experimental setup used to generate the impulse load of the granular medium.

setup is shown in Fig. 1. It consists of the thick wall cylinder with an inner diameter of 60 mm mounted on a massive metal plate, a piston of mass 1.538 kg, and a plunger of mass 1.394 kg, all made of steel. The cylinder is filled with the steel spherical beads of 3 ± 0.01 mm diameter. The plunger moves along the guides to impact the piston, generating an impulse load of stress exerted on the granular medium. To smooth the impulse loading, a rubber gasket located at the top surface of the piston is used. The gasket also is used to suppress high frequency parasitic oscillations in transverse directions due to unavoidable roughness of the plunger's surface or a small deviation of the plunger from the perfectly vertical direction of motion. The piston consists of two parts with the thinner 3 mm thick part being in contact with the sample.

The sample sandwiched by these two parts measures the total force acting on the granular sample. Both parts of the piston move along the guides to establish the one-dimensional motion of the piston, its displacement being recorded by a photosensor. At the bottom of the cylinder three smaller pistons with diameters of 3 mm are mounted to transmit the load from the beads to the sensors. This setup allows one to measure the normal force experienced by a single bead at the bottom of the granular sample.

The piston-sensor assemblies are located at different distances at 10, 20, and 30 mm from the inner vertical wall of the cylinder. The experimental set comprises 250 runs, each involving impact of the granular sample by the plunger dropped from the height of 0.5 m to exclude the plastic deformations of particles at higher heights. The granular sample for each run is prepared by placing 7223 beads into the cylinder, followed by their compaction by the piston to achieve the same initial volume and grain density. For each individual run, three records of the time evolution of the forces were recorded using piston sensors, resulting in 750 force vs time records.

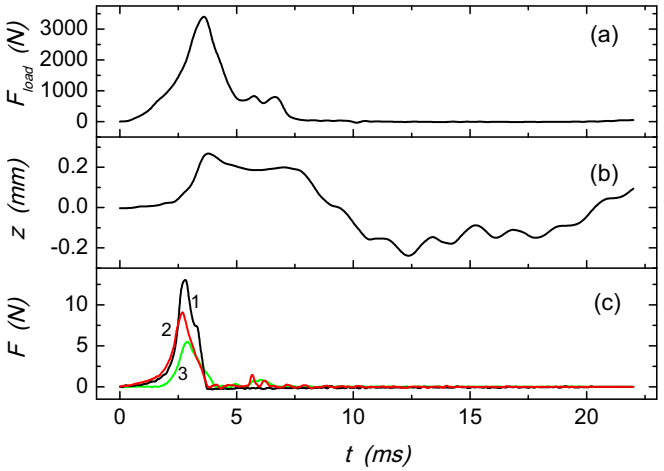

FIG. 2. Time dependence of (a) the force exerted by the piston on the granular medium, (b) the displacement of the piston, and (c) the corresponding forces exerted on the piston sensors.

III. EXPERIMENTAL RESULTS

The typical time dependence of the driving force, displacement of the piston, and force on a grain measured by the piston sensors at the bottom of the sample are shown in Fig. 2. A set of 250 $F(t)$ records, averaged over three sensors at the bottom of the sample, is used to build the force distribution, shown in Fig. 3, by reading the maximum force at the maximum of the impulse $F(t)$, see Fig. 2. The dimensionless force f is the force F normalized by the mean force: $f = F/\langle F \rangle$. For large forces $f > 1$, the distribution function P is of exponential form

$$P \propto e^{-\beta f}, \qquad f > 1, \tag{1}$$

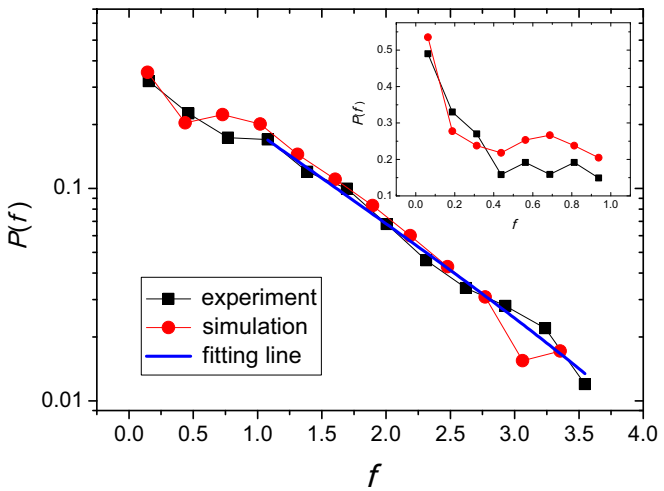

FIG. 3. The probability density P of maximum dimensionless forces f exerted on the grains at the bottom of the sample measured in the experiment and compared to that obtained from simulation. The inset shows small force distributions. The experimental data are averaged over all three sensors. The exponential fit of experimental data by expression (1) is shown as well.

where exponent β is 1.0 ± 0.1, see the fitting line in Fig. 3. The coefficient β is less than that found in static experiments $\beta = 1.1$–1.8 where glass beads were used [2,3,15,16]. The small force distributions $f < 1$ shown in the inset are different from those for large forces $f > 1$. Here we have used a smaller binning width to obtain more accurate distribution in this area.

IV. COMPUTER SIMULATIONS

Simulation of dynamical loading of the granular samples is performed to gain insight into the response of the granular sample to the dynamical loading not only at the bottom of the sample as in experiment, but also throughout the volume of the medium. The discrete element method, originally developed by Cundall and Strack [39], is used to obtain force distributions. The simulation setup closely follows the experiment by using the same particles' size and shape. The interparticle interactions are described by the Hertzian law and the friction—by the Coulomb model. The friction coefficient $\mu = 0.1$ was measured experimentally in this paper using a method proposed by Blair *et al.* [2]. The elastic properties of the steel beads are described by the steel's Young's modulus $E = 211.0$ GPa and the Poisson ratio $\nu = 0.32$. The dynamic loading of the sample is simulated by using experimental force vs time $F_{\text{load}}(t)$ dependence exerted on the granular sample by the piston. This dependence represented by the maximum force $\langle F_{\text{load}\,m} \rangle = 3450$ N and the width $\langle \tau_{\text{load}} \rangle = 1.65$ ms obtained from all 250 measurements described above is presented in Fig. 2(a).

The series of ten simulations are performed for different initial packings of a granular massif with the height of $h = 61.7$ mm, which is the same as in the experiment. The direct simulation of the granular response to drop weight would not provide a proper comparison between simulation and experiment. The complication arises from the presence of the rubber gasket used in experiment resulting in a complex response, which is difficult to reproduce in simulations. Therefore, to provide a meaningful comparison between experiment and simulations, the time-dependent force $F_{\text{load}}(t)$ measured in experiment is used as the driving stimulus in the simulations. The average number of particles at the bottom of the cylindrical container is 248. As in the experiment, the time dependence of forces acting at the bottom of the sample displays a pronounced maximum. The calculated maximum force distribution is in good agreement with experiment, see Fig. 3, the exponent β in the part of the distribution for large forces $f > 1$ being 1.04 ± 0.15.

The distribution of interparticle maximum forces $P(f)$ in the interior of the sample also is calculated and shown in Fig. 4(a). The exponential decay of $P(f)$ at large forces ($f > 1$) is more pronounced compared to that measured at the bottom of the sample (Fig. 3), the exponent being $\beta = 1.70 \pm 0.02$. The simulation also allows us to obtain the evolution of the force distribution with time, see Fig. 4(b). There is a slight time dependence of the distribution, but more importantly, all of the distributions obtained at different times exhibit exponential decay, which results from large-scale correlations existing in the system. If it was not the case, the Gaussian distribution would be observed in the absence of the correlations. The dependence of coefficient β on time is presented in Fig. 5(a). To assess the deviation from exponential dependence, the force distributions are fitted using the exponent of the quadratic function of f: $P'(f) = \exp(\alpha - \beta f + \gamma f^2)$ where the quadratic term γf^2 is responsible for the deviation. The results of fitting show that the coefficient γ is small for the entire duration of the impulse loading, see Fig. 5(b).

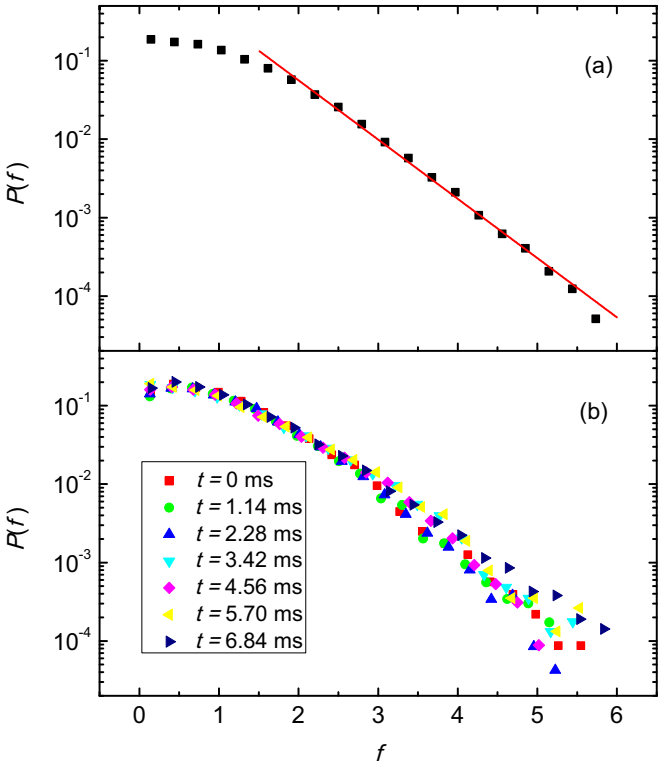

FIG. 4. (a) Probability density $P(f)$ of maximum interparticle forces in interior of the granular sample. The exponential fit of $P(f)$ for large forces $f > 1$ is shown as the straight line; (b) probability density $P(f)$ at various times 0, 1.14, 2.28, 3.42, 4.56, 5.70, and 6.84 ms.

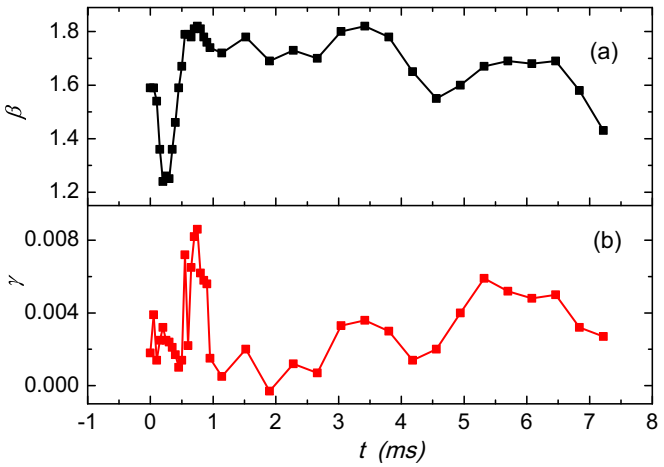

FIG. 5. (a) The exponent β of large-force distribution in the bulk of the sample; (b) the coefficient γ in the square term responsible for deviation on exponential dependence at various times.

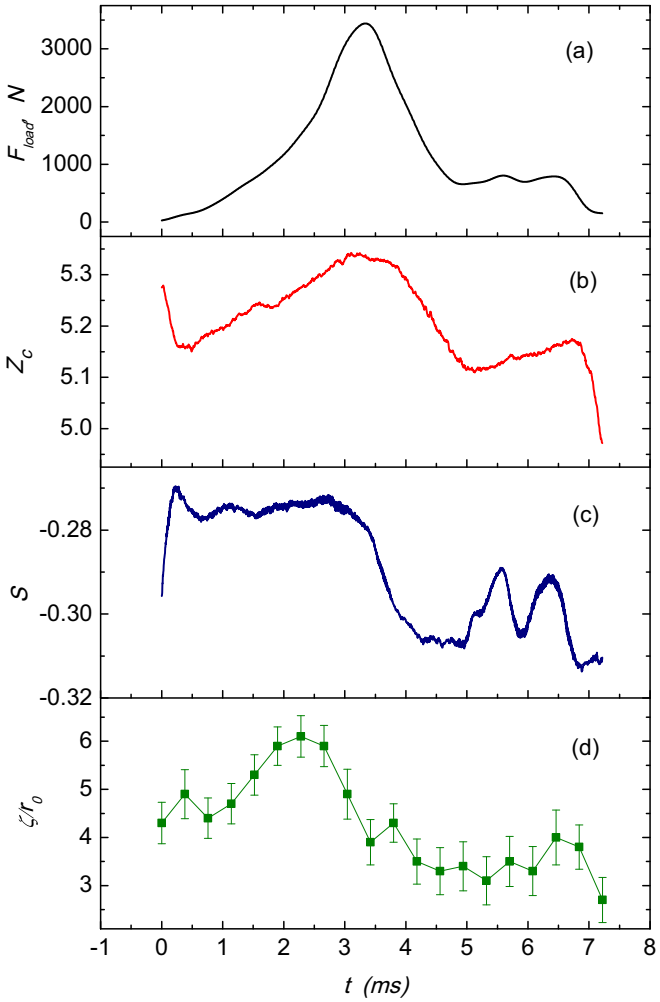

FIG. 6. Time dependence of (a) loading force F_{load}, (b) coordination number Z_c, (c) orientational order parameter S, and (d) reduced correlation radius ζ/r_0.

To study the time evolution of the correlation properties of the granular system, the following correlation function is calculated:

$$C(r) = \frac{\langle F_{ik}F_{jl}\delta(\mathbf{r}_i - \mathbf{r}_j - \mathbf{r})\rangle - \langle F_{ik}\rangle\langle F_{jl}\rangle}{\langle F_{ik}\rangle\langle F_{jl}\rangle}, \qquad (2)$$

where F_{ij} is the absolute value of the force exerted on the ith particle by the kth particle, $\mathbf{r}_i$ is the radius vector of the ith particle, and the averaging is performed over particles located at the distances $l > 4r_0$ from the wall to avoid its influence (r_0 is the average radius of the grains). The correlation radius ζ is obtained from $C(r)$ as

$$C(r) \propto e^{-r/\zeta}. \qquad (3)$$

The calculated correlation radii ζ as a function of time shown in Fig. 6(d) demonstrates that its changes are not completely in synchronization with the varying load. Figure 6(c) also displays the time dependence of the average coordination number Z_c and the orientational order parameter S, which determines the average orientation of the interparticle forces.

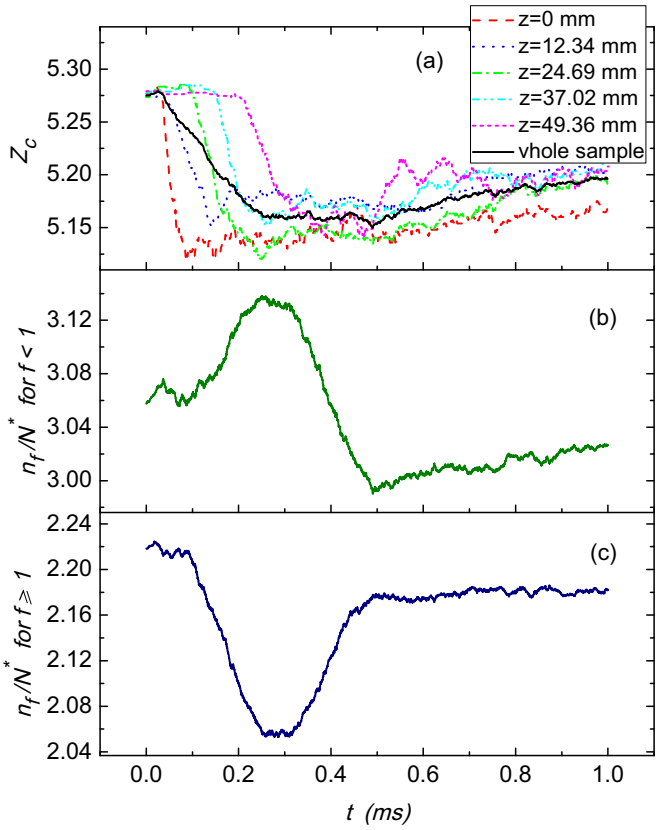

FIG. 7. (a) Time dependence of coordination number Z_c at five locations along the direction of the wave propagation (z is the distance from the piston) as well as averaged over the entire sample. (b) Relative number of small forces and (c) relative number of large forces calculated using N^*—the number of particles that are not in contact with the walls.

S is calculated following the procedure in Ref. [40],

$$S = \frac{2}{L}\sum_i l_i^2 \cos^2\theta_i - 1, \qquad (4)$$

where l_i is the distance between centers of two contacting particles, θ_i is the angle between the interparticle force and the vertical line, and $L = \sum_i l_i^2$ is the total square length of interparticle distances l_i. The parameter $S = 1$ if all forces are vertical, $S = 0$ if forces are randomly oriented or all directed at 45°, and $S = -1$ if forces are horizontally oriented.

The time dependence of average coordination number Z_c on time is very similar to that of loading force F_{load}, except for the interval $t < 0.5$ ms at the beginning of the loading process, where Z_c decreases sharply, in contrast to a gradual increase in F_{load}. In addition, both orientational order parameter S and exponent β change significantly. As a compaction wave propagates from the driving piston inside the sample, it breaks the balance resulting in a reduced number of neighbor particles as well as the average coordination number. The time dependence of the local coordination number measured in several points along the sample demonstrates a sharp reduction of Z_c over time, see Fig. 7(a), whereas its average over the entire sample changes more gradually. Comparing $Z_c(t)$ at various localizations, we can make the conclusion that

at $t > 0.4$ ms the coordination number is distributed almost uniformly over the sample. Figure 7, panels (b) and (c) display the time dependence of the relative number of small and large forces: It is obvious that the number of large interparticle forces decreases and the number of small particles increases resulting in the partial disappearance of a strong subnetwork. These observations indicate that the granular medium is changing its internal packing structure at the beginning of the loading. The fact that the time dependence of the major parameters characterizing the microstructure of the sample does not follow the time evolution of the loading force clearly demonstrates the nonequilibrium response of the granular system subjected to dynamic loading.

V. CONCLUSIONS

To summarize, this paper presents a joint experimental and theoretical investigation of the force distribution in the cylindrical granular medium subjected to an impulse load. The original experimental setup was devised to measure the local distribution of the forces at the bottom of the sample. It was found that for large forces ($f > 1$) the distribution function attenuates exponentially, similar to that measured in static experiments, but with a smaller exponent β. By performing discrete element method simulations under experimental conditions, good agreement between experimental and simulated maximum force distributions at the bottom of the sample is found. The simulations also provide additional details not available from experiment, including the time evolution of the probability density inside the granular medium as well as the spatial correlation radii as a function of time. The distribution functions of the interparticle forces inside the sample, as shown in simulation, also decay exponentially at all times during the loading process. The time evolution of the parameters characterizing the microstructure of the granular medium (coordination number Z_c, orientational order parameter S, correlation radius ζ, and force distribution exponent β) during the dynamic loading clearly indicate the nonequilibrium nature of the deformation response.

ACKNOWLEDGMENTS

This research was supported by the National Academy of Sciences of Ukraine, Grant No. 0113U000008 and the Defense Threat Reduction Agency, Grant No. HDTRA1- 12-1-0023.

[1] D. Howell, R. P. Behringer, and C. Veje, Phys. Rev. Lett. **82**, 5241 (1999).
[2] D. L. Blair, N. W. Mueggenburg, A. H. Marshall, H. M. Jaeger, and S. R. Nagel, Phys. Rev. E **63**, 041304 (2001).
[3] J. M. Erikson, N. W. Mueggenburg, H. M. Jaeger, and S. R. Nagel, Phys. Rev. E **66**, 040301 (2002).
[4] C. H. Liu, S. R. Nagel, D. A. Schecter, S. N. Coppersmith, S. Majumdar, O. Narayan, and T. A. Witten, Science **269**, 513 (1995).
[5] J. Duran, *Sands, Powders, and Grains: An Introduction to the Physics of Granular Materials* (Springer, New York, 2000).
[6] R. Behringer, D. Howell, L. Kondic, S. Tennakoon, and C. Veje, Physica D **133**, 1 (1999).
[7] T. S. Majmudar and R. P. Behringer, Nature (London) **435**, 1079 (2005).
[8] I. Zuriguel and T. Mullin, Proc. R. Soc. London, Ser. A **464**, 99 (2008).
[9] J. Zhang, T. S. Majmudar, A. Tordesillas, and R. P. Behringer, Granular Matter **12**, 159 (2010).
[10] L. Zhang, Y. Wang, and J. Zhang, Phys. Rev. E **89**, 012203 (2014).
[11] F. Radjai, M. Jean, J.-J. Moreau, and S. Roux, Phys. Rev. Lett. **77**, 274 (1996).
[12] F. Radjai, S. Roux, and J. J. Moreau, Chaos **9**, 544 (1999).
[13] J. H. Snoeijer, M. van Hecke, E. Somfai, and W. van Saarloos, Phys. Rev. E **67**, 030302 (2003).
[14] G. Lois, A. Lemaître, and J. M. Carlson, Phys. Rev. E **76**, 021302 (2007).
[15] D. M. Mueth, H. M. Jaeger, and S. R. Nagel, Phys. Rev. E **57**, 3164 (1998).
[16] G. Lovoll, K. J. Maloy, and E. G. Flekkoy, Phys. Rev. E **60**, 5872 (1999).
[17] B. Miller, C. O'Hern, and R. P. Behringer, Phys. Rev. Lett. **77**, 3110 (1996).
[18] S. J. Antony, Phys. Rev. E **63**, 011302 (2000).
[19] H. A. Makse, D. L. Johnson, and L. M. Schwartz, Phys. Rev. Lett. **84**, 4160 (2000).
[20] L. E. Silbert, G. S. Grest, and J. W. Landry, Phys. Rev. E **66**, 061303 (2002).
[21] F. Radjai, D. E. Wolf, M. Jean, and J.-J. Moreau, Phys. Rev. Lett. **80**, 61 (1998).
[22] S. N. Coppersmith, C.-h. Liu, S. Majumdar, O. Narayan, and T. A. Witten, Phys. Rev. E **53**, 4673 (1996).
[23] M. Nicodemi, A. Coniglio, and H. J. Herrmann, J. Phys. A **30**, L379 (1997).
[24] J.-P. Bouchaud, P. Claudin, D. Levine, and M. Otto, Eur. Phys. J. E **4**, 451 (2001).
[25] A. H. W. Ngan, Proc. R. Soc. London, Ser. A **461**, 1423 (2005).
[26] S. Henkes and B. Chakraborty, Phys. Rev. E **79**, 061301 (2009).
[27] N. Iikawa, M. M. Bandi, and H. Katsuragi, J. Phys. Soc. Jpn. **84**, 094401 (2015).
[28] Y. Zhou, R. D. Wildman, and J. M. Huntley, Proc. R. Soc. London, Ser. A **466**, 789 (2009).
[29] Y. H. Wang and Y. Gao, Granular Matter **16**, 55 (2014).
[30] Y.-H. Wang, M. Asce, Y. Gao, and G. Leng, J. Geotech. Geoenviron. Eng. **142**, 06015016 (2015).
[31] M. P. Ciamarra, A. H. Lara, A. T. Lee, D. I. Goldman, I. Vishik, and H. L. Swinney, Phys. Rev. Lett. **92**, 194301 (2004).
[32] R. C. Hurley, K.-W. Lim, and J. E. Andrade, in *Rapid Penetration into Granular Media: Visualizing the Fundamental Physics of Rapid Earth Penetration*, edited by M. Iskander, S. Bless, and M. Omidvar (Elsevier Amsterdam, 2015).
[33] J. Brujić, S. F. Edwards, I. Hopkinson, and H. A. Makse, Physica A **327**, 201 (2003).
[34] A. D. D. J. Zhou, S. Long, and Q. Wang, Science **312**, 1631 (2006).

[35] S. Mukhopadhyay and J. Peixinho, Phys. Rev. E **84**, 011302 (2011).
[36] N. Brodu, J. A. Dijksman, and R. P. Behringer, Nat. Commun. **6**, 6361 (2015).
[37] M. Saadatfar, A. P. Sheppard, T. J. Senden, and A. J. Kabla, J. Mech. Phys. Solids **60**, 55 (2012).
[38] R. C. Hurley, S. A. Hall, J. E. Andrade, and J. Wright, Phys. Rev. Lett. **117**, 098005 (2016).
[39] P. A. Cundall and O. D. L. Strack, Géotechnique **29**, 47 (1979).
[40] N. Iikawa, M. M. Bandi, and H. Katsuragi, Phys. Rev. Lett. **116**, 128001 (2016).